THE JOURNAL OF PHYSICAL CHEMISTRY B

Article

pubs.acs.org/JPCB

Combination of MD Simulations with Two-State Kinetic Rate Modeling Elucidates the Chain Melting Transition of Phospholipid Bilayers for Different Hydration Levels

Bartosz Kowalik,[†] Thomas Schubert,[‡] Hirofumi Wada,[§] Motomu Tanaka,[‡,∥] Roland R. Netz,[†] and Emanuel Schneck*[,⊥]

[†]Fachbereich Physik, Freie Universität Berlin, D-14195 Berlin, Germany

[‡]Institute of Physical Chemistry, Heidelberg University, D-69120 Heidelberg, Germany

[§]Department of Physics, Ritsumeikan University, Kusatsu, 525-8577 Shiga, Japan

[∥]Institute for Integrated Cell-Material Sciences (WPI iCeMS), Kyoto University, 606-8501 Kyoto, Japan

[⊥]Biomaterials Department, Max Planck Institute of Colloids and Interfaces, D-14476 Potsdam, Germany

Supporting Information

ABSTRACT: The phase behavior of membrane lipids plays an important role in the formation of functional domains in biological membranes and crucially affects molecular transport through lipid layers, for instance, in the skin. We investigate the thermotropic chain melting transition from the ordered L_β phase to the disordered L_α phase in membranes composed of dipalmitoylphosphatidylcholine (DPPC) by atomistic molecular dynamics simulations in which the membranes are subject to variable heating rates. We find that the transition is initiated by a localized nucleus and followed by the propagation of the phase boundary. A two-state kinetic rate model allows characterizing the transition state in terms of thermodynamic quantities such as transition state enthalpy and entropy. The extrapolated equilibrium melting temperature increases with reduced membrane hydration and thus in tendency reproduces the experimentally observed dependence on dehydrating osmotic stress.

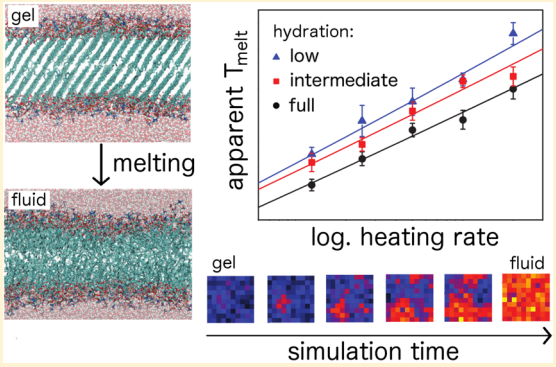

INTRODUCTION

One main structural component of biological membranes is the lipid bilayer.[1] Membrane lipids self-assemble into a rich variety of supramolecular architectures, depending on the lipid chemical structure, lipid composition, thermodynamic parameters like temperature and pressure, and other influences.[2,3] This variability is essential for biological functionality, as it allows, for instance, for the transient formation of functional lipid domains in biomembranes.[4] The phase behavior of lipid membranes plays an important role in this context, because domain formation is promoted by the lipids' tendency to assume phases with crystal-like ordering[5] at low temperature and low hydration. Ordered and disordered membrane phases also exhibit substantially different permeability for molecular transport in general and for water in particular.[6]

For phospholipids, an important class of membrane lipids, the phase behavior has been extensively studied experimentally. The experiments revealed that lipids with saturated alkyl chains and zwitterionic phosphatidylcholine (PC) headgroups undergo a thermotropic phase transition between the L_β phase, in which the chains assume crystalline distorted-hexagonal ordering, and the fluid L_α phase, in which chains are disordered and lipids are laterally highly mobile within the bilayer. This transition is known as the *chain melting transition*. For simulation snapshots of lipid bilayers in the L_β and L_α phases see Figure 1. In the L_β phase the alkyl chains assume so-called all-trans and thus essentially linear conformations (Figure 1, left). In contrast, the key structural manifestation of the L_α phase is a considerable density of gauche bonds, allowing the alkyl chains to assume more random configurations (Figure 1, right). Both phases have been structurally characterized by small- and wide-angle X-ray scattering experiments,[7−9] and differential scanning calorimetry (DSC) revealed the equilibrium transition temperature as well as enthalpy and entropy differences between L_α and L_β phases.[10−12] It was found that the phase behavior of phospholipid membranes is significantly influenced by osmotic dehydration,[13−15] which has far-reaching consequences for tissues exposed to variable humidity levels, such as the skin.[6] In fact, the working principle of so-called

Received: June 9, 2015
Revised: October 5, 2015
Published: October 6, 2015

DOI: 10.1021/acs.jpcb.5b05501
J. Phys. Chem. B 2015, 119, 14157−14167

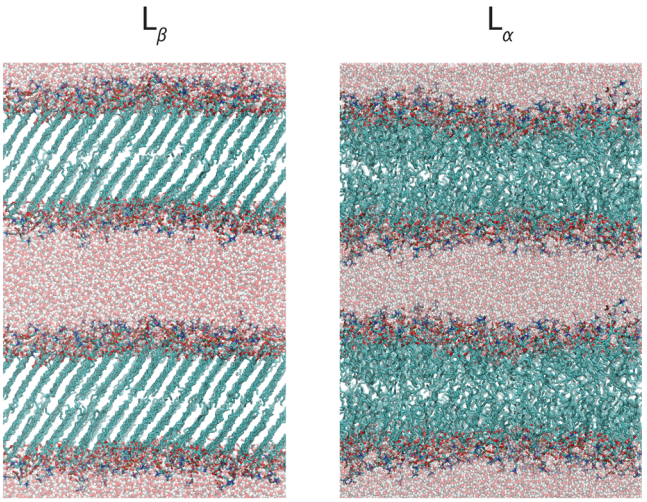

Figure 1. Simulation snapshots of bilayers composed of 288 DPPC lipids hydrated with n_w = 31 water molecules per lipid in the L_β phase (left) and in the L_α phase (right). This high hydration level approximates isolated, noninteracting bilayers. The simulation box contains one hydrated bilayer membrane with periodic boundary conditions in *x*, *y*, and *z* directions; in the snapshots we duplicate the simulation box in *z* direction to visualize finite-size effects.

moisturizers is closely related to this phenomenon and the object of current research.[16]

The chain melting transition of lipid membranes has been discussed within the general framework of solid/liquid phase coexistence,[17−21] and elaborate models predicting differences in the thermodynamic properties of the two phases, based on molecular interactions and configurational entropy, have been developed.[22−24] However, little is known about the melting kinetics and in particular the structural and thermodynamical properties of the transition state. The direct experimental observation of transition states is difficult, although experiments have yielded an indirect estimate of the minimum nucleation domain size under conditions of L_α and L_β phase coexistence.[18]

Detailed information on the behavior of complex molecular systems is in principle contained in molecular dynamics (MD) simulations. To date, atomically resolved molecular dynamics simulations of phospholipid bilayers in the fluid L_α phase have successfully reproduced experimental results in various structural, dynamical, and thermodynamical aspects.[25−28] Some studies were aimed at reproducing the structural features of L_β phases by annealing L_α phase bilayers below the chain melting temperature. This turned out to be difficult within the simulation time scale, and "quenched" structures were frequently obtained.[29,30] L_β phase simulations therefore mostly rely on prearranged L_β structures based on crystallography data.[31−33] Recently, an "assisted freezing" method was reported that enables generating L_β phases with a minimum amount of a priori information, whose structural and thermodynamical properties are in good agreement with experiments.[30] Using this method, the sharp thermotropic phase transition of dipalmitoylphosphatidylcholine (DPPC) from L_β to L_α phase upon heating was reproduced, with a transition enthalpy in good agreement with experiments. For the same lipid, Coppock et al.[33] determined the phase transition temperature in simulations of bilayers composed of coexisting prearranged L_α and L_β regions. Thus far, the influence of dehydration on the L_β to L_α transition has not been considered in atomistic simulations.

It is generally difficult to identify transition states in MD simulations. Structural features of newly formed nuclei are typically not easily recognized,[34] and simulation time scales often do not allow for a quasi-static variation of the phase-determining control parameters. Moreover, MD simulations only yield system energies directly; for free energies more involved techniques must be used. While such methods are commonly employed in cases where the relevant reaction coordinate is a spatial one and corresponds to the separation between two atoms or molecules,[35] they are not directly applicable to thermotropic phase transitions like the chain melting transition of lipid membranes.

In the present study we investigate the thermotropic chain melting transition of DPPC by atomistic MD simulations. The trajectories are interpreted with a two-state kinetic rate model which enables estimation of the thermodynamic properties and the size of the transition nucleus. Using this approach we elucidate the influence of the hydration level on the chain melting transition. To this end we study membranes hydrated with n_w = 31, 10, and 7 water molecules per lipid. For the highest hydration level (n_w = 31) the simulations to good approximation represent isolated lipid membranes, realized for instance with large unilamellar vesicles. The theoretical concepts introduced are generally applicable to thermotropic first-order phase transitions in computer simulations and may therefore find use for the investigation of transition states in solid−liquid transitions,[34] cooperative helix−coil transitions, and thermal protein unfolding as well.[36−38]

MATERIALS AND METHODS

The simulation box contains either N_l = 288 or N_l = 72 DPPC molecules forming a single lipid bilayer in water with $N_l/2$ molecules per membrane leaflet. DPPC is a zwitterionic phospholipid which carries no net charge. The membrane is arranged parallel to the (*x*,*y*) plane without any position restraints and stabilized by the hydrophobic effect. Periodic boundary conditions in *x*, *y*, and *z* directions are applied. Simulations are performed with the GROMACS software package.[39] The OPLS (optimized potentials for liquid simulations)-based united-atom lipid force field and DPPC force field[40−42] are used in combination with TIP3P water.[43] To reduce calculation time and in order to stay consistent with our previous work,[30] H-angle restraints and a time step of 0.004 ps are used. Simulations are run with anisotropic pressure coupling at 1 bar using the Berendsen barostat with a time constant of τ_P = 0.5 ps. Temperature is controlled with the Berendsen thermostat[44] with a time constant of τ_T = 0.1 ps. We use a plain Lennard−Jones cutoff of 1.0 nm and account for electrostatic interactions using the particle mesh Ewald (PME) method[45,46] with a 1.0 nm real-space cutoff. The initial L_β structure is equilibrated for 25 ns at T = 310 K prior to production runs. Heating scans are performed by single continuous runs, with constant heating rates as described in the text. System enthalpies are extracted from the simulation trajectories by monitoring potential and kinetic energies while explicitly accounting for the volumetric contribution PV, although the latter contributes negligibly at 1 atm. A gauche bond is defined as a bond whose dihedral angle is larger than 90°. Since the distribution of the dihedral angles exhibits two clearly separated peaks around 0° (trans) and 120° (gauche) with almost zero occupation around 90°, this provides a sharp distinction between gauche and trans bonds. The average number of gauche dihedrals per lipid in a unit volume is

DOI: 10.1021/acs.jpcb.5b05501
J. Phys. Chem. B 2015, 119, 14157−14167

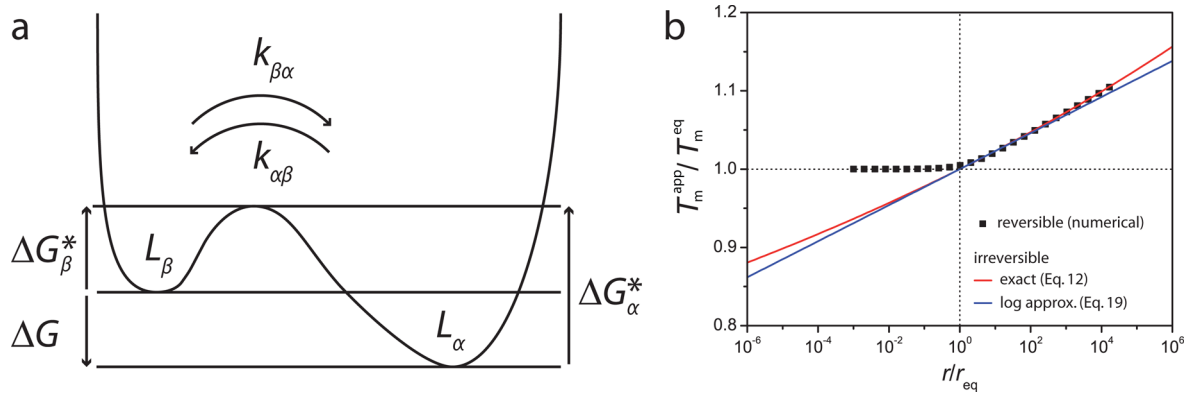

Figure 2. (a) Two-state kinetic rate model used to interpret the heating rate dependence of apparent chain melting temperatures in the MD simulations. (b) Apparent chain melting temperature as a function of the reduced heating rate, r/r_{eq}, as predicted by the two-state model according to different approximations. For high heating rates the melting is essentially irreversible ($k_{\alpha\beta} \approx 0$).

computed by counting the gauche dihedrals in a certain volume and subsequent division by the (fractional) number of lipids in this volume.

RESULTS

In earlier work it was demonstrated that hydrated L_β phases of DPPC generated by an assisted freezing method assume structural properties consistent with experiments.[30] In that study also the enthalpy change per lipid accompanying the phase transition from L_β to L_α, Δh, was found to be in reasonable agreement with calorimetry experiments. In the present work, we investigate the nature of the transition state and study the dependence on the lipid hydration level. For this purpose, hydrated DPPC membranes in L_β phase were first equilibrated at T_{init} = 310 K and then heated at various heating rates r ranging from 0.125 to 2 K/ns. Figure 1 shows representative simulation snapshots of bilayers in the L_β phase (left) and L_α phase (right). Here, each simulation box has periodic boundary conditions in x, y, and z directions and contains one bilayer composed of N_l = 288 lipids and hydrated with n_w = 31 water molecules per lipid. This hydration level is so high that the systems to good approximation represent isolated lipid membranes, realized for instance with large unilamellar vesicles. In our simulations we also consider lower hydration levels of n_w = 10 and 7 (see section Influence of the Hydration Level).

Two-State Kinetic Rate Model of Membrane Melting. Figure 2a illustrates the two-state kinetic model employed for the description of the phase transition between the ordered L_β and the fluid L_α phase in a bilayer system. ΔG denotes the free-energy difference for a finite system size between the L_β and the L_α phase

$$\Delta G = \Delta H - T\Delta S \tag{1}$$

where ΔH and ΔS denote transition enthalpy and transition entropy, respectively. Both quantities are assumed as temperature independent. By definition, ΔG is zero at the equilibrium phase transition temperature T_m^{eq}, thus

$$T_m^{eq} = \Delta H/\Delta S \tag{2}$$

ΔG^*_α and ΔG^*_β in Figure 2a denote the free-energy barrier heights with respect to the L_α and L_β phases

$$\Delta G^*_\beta = \Delta H^*_\beta - T\Delta S^*_\beta \tag{3}$$

$$\Delta G^*_\alpha = \Delta H^*_\alpha - T\Delta S^*_\alpha = \Delta H^*_\beta - \Delta H - T(\Delta S^*_\beta - \Delta S) \tag{4}$$

where $\Delta G^*_\alpha = \Delta G^*_\beta - \Delta G$ is used (see Figure 2a). In a simple Arrhenius description the transition rates between the two states over the barrier, $k_{\beta\alpha}$ and $k_{\alpha\beta}$, are given as

$$k_{\beta\alpha} = k_0 e^{-\Delta G^*_\beta/k_B T} \tag{5}$$

$$k_{\alpha\beta} = k_0 e^{-\Delta G^*_\alpha/k_B T} \tag{6}$$

where k_0 denotes a prefactor representing the transition attempt frequency, which must be identical since $k_{\beta\alpha}/k_{\alpha\beta} = e^{-\Delta G/k_B T}$.

The relative fractions by which the L_α and L_β states are populated in an ensemble are denoted with f_α and f_β, with $f_\beta + f_\alpha = 1$. In the following, a linear temperature increase with time t is considered

$$T(t) = T_{init} + rt \tag{7}$$

For mathematical convenience we define the apparent melting time t_m via the steepest decrease in the occupation of the ordered state

$$(d^2 f_\beta/dt^2)_{t_m} = 0 \tag{8}$$

The apparent melting temperature then is simply

$$T_m^{app}(r) = T_{init} + rt_m \tag{9}$$

Reversible Melting. The fraction f_β obeys the first-order rate equation

$$df_\beta/dt = -f_\beta k_{\beta\alpha}(t) + f_\alpha k_{\alpha\beta}(t) \tag{10}$$

which in conjunction with eqs 3−7 has no closed-form solution. Accordingly, $T_m^{app}(r)$ can only be obtained by numerical evaluation of eqs 8−10. The result for $\Delta H^*_\beta/(k_B T_m^{eq}) = 100$ is shown exemplarily in Figure 2b (symbols) in terms of the reduced temperature T_m^{app}/T_m^{eq} as a function of the reduced heating rate r/r_{eq}: For slow heating rates, i.e., close to thermal equilibrium, we find $T_m^{app}(r) \approx T_m^{eq}$. For fast heating above a characteristic heating rate r_{eq} (which will be defined below), $T_m^{app}(r)$ increases approximately logarithmically with the heating rate.

Irreversible Melting. When melting is assumed to be irreversible ($k_{\alpha\beta} = 0$) we are left with the simple homogeneous rate equation

DOI: 10.1021/acs.jpcb.5b05501
J. Phys. Chem. B 2015, 119, 14157−14167

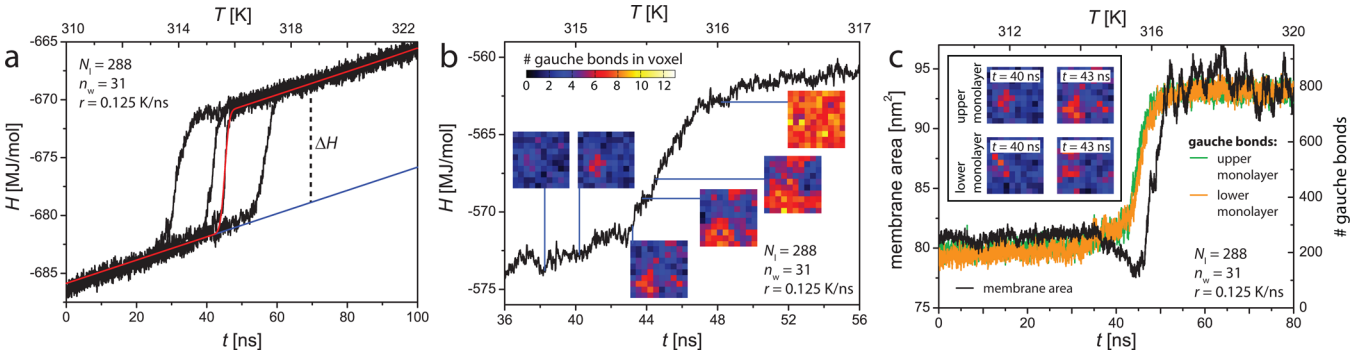

Figure 3. (a) System enthalpies H (black lines) in four independent representative heating simulations of a large bilayer (N_l = 288) at the highest hydration (n_w = 31) at heating rate r = 0.125 K/ns as a function of the simulation time t (lower axis) and of the instantaneous temperature T (upper axis). The red line is the fit to one curve according to eq 20. The solid blue line is the linear baseline. ΔH is the total phase transition enthalpy. (b) Evolution of the system enthalpy in the fitted run around the transition. (Insets) Density of alkyl chain gauche bonds in one membrane monolayer as a function of the x and y coordinates in the membrane plane at selected simulation times. (c) Number of alkyl chain gauche bonds in the lower (orange line) and upper (green line) lipid monolayer around the transition. The black line indicates the evolution of the membrane area. (Inset) Comparison between gauche bond densities in upper and lower monolayers at selected simulation time points during the early stage of the transition.

Table 1. Equilibrium Chain Melting Temperatures T_m^{eq} and Their Incremental Shift ΔT_m^{eq} upon Dehydration with Respect to the Highest Hydration, as Well as Transition Enthalpies and Transition Entropies As Deduced from the Simulations at Various Hydration Levels n_w and System Sizes Characterized by the Number of Lipids N_l

N_l	n_w	T_m^{eq} [K][a]	ΔT_m^{eq} [K]	ΔH [MJ/mol]	Δh [kJ/mol][b]	ΔS [kJ/(mol K)]	Δs [J/(mol K)]
288	7	313.1 ± 1.6	1.6 ± 0.9	11.2 ± 0.1	39.0 ± 0.2	35.9 ± 0.2	125 ± 1
288	10	312.6 ± 1.5	1.2 ± 0.9	11.3 ± 0.1	39.3 ± 0.3	36.2 ± 0.3	126 ± 1
288	31	311.5 ± 1.4	0.0	10.7 ± 0.1	37.0 ± 0.3	34.2 ± 0.3	119 ± 1
72	31	311.5 ± 3.5		2.4 ± 0.1	33.1 ± 0.8	7.6 ± 0.5	106 ± 7

[a]Experimental value at excess hydration: $T_m^{eq} \approx 315$ K (e.g., 314.4[15] and 315.6 K[59]). [b]Experimental value of the $L_\beta \rightarrow L_\alpha$ enthalpy difference: $\Delta h \approx$ 41−46 kJ/mol (e.g., 43[54] and 44 kJ/mol[11]).

$$df_\beta/dt = -f_\beta k_{\beta\alpha} \tag{11}$$

for which $T_m^{app}(r)$ is obtained algebraically (see Supporting Information) as

$$T_m^{app}(r) = \theta\cdot[2W(\sqrt{r^*/r})]^{-1} \tag{12}$$

with $\theta = \Delta H_\beta^*/k_B$ and $r^* = k_0 \Delta H_\beta^* e^{\Delta S_\beta^*/k_B}/(4k_B)$. Equation 12 is an equivalent representation of the well-known Kissinger relation between reaction temperatures and the heating rate.[47,48] $W(x)$ denotes the principal branch of the Lambert W function.[49] $T_m^{app}(r)$ for irreversible melting according to eq 12 is plotted in Figure 2b as a solid red line. It matches the numerical result for reversible melting in the limit of fast heating for $r \gg r_{eq}$. One has $T_m^{app} = T_m^{eq}$ for the characteristic heating rate

$$r_{eq} = r^*\left(\frac{\theta}{2T_m^{eq}} e^{\theta/2T_m^{eq}}\right)^{-2} \tag{13}$$

as follows from the defining property of the Lambert W function, $W(xe^x) = x$.

The scaling parameters θ and r^* define the transition state, characterized by ΔH_β^* and ΔS_β^* (see eq 3), via the relations

$$\Delta H_\beta^* = k_B\theta \tag{14}$$

$$\Delta S_\beta^* = k_B \ln\left(\frac{4r^*}{k_0\theta}\right) \tag{15}$$

As shown in the Supporting Information, $T_m^{app}(r)$ can be approximated logarithmically in the vicinity of an arbitrarily chosen reference heating rate r_0

$$T_m^{app}(r) \approx T_0 + C \ln\left(\frac{r}{r_0}\right) \tag{16}$$

with

$$T_0 = \theta\cdot[2W(\sqrt{r^*/r_0})]^{-1} \tag{17}$$

and

$$C = \theta\cdot[4W(\sqrt{r^*/r_0})(1 + W(\sqrt{r^*/r_0}))]^{-1} \tag{18}$$

Note that both T_0 and C are functions of the scaling parameters θ and r^* for a given reference heating rate r_0. The logarithmic result is analogous to the rupture force of single bonds that shows a logarithmic loading rate dependence.[50−52] In that case the free energy difference between bound and free states depends linearly on the loading rate. Here, the exact solution (eq 12) has a more complicated structure involving the Lambert W function because time enters the temperature which appears in the denominator of the exponential factor in the rate equation. As further shown in the Supporting Information, eq 16 can be rewritten in the form

$$T_m^{app}(r) \approx T_m^{eq} + \frac{T_m^{eq2}}{\theta} \ln\left(\frac{r}{r_{eq}}\right) \tag{19}$$

DOI: 10.1021/acs.jpcb.5b05501
J. Phys. Chem. B 2015, 119, 14157−14167

for the particular choice $r_0 = r_{eq}$, where $T_m^{app} = T_m^{eq}$, see eqs 16 and 13. This logarithmic approximation around r_{eq} is indicated in Figure 2b by a solid straight blue line.

General Aspects of the Melting Process. Figure 3a shows the evolution of the system enthalpy $H = U + PV$ in four independent representative heating simulations of a bilayer with $N_l = 288$ lipids at the highest hydration ($n_w = 31$) and a heating rate $r = 0.125$ K/ns as a function of the simulation time (lower axis) and of the instantaneous temperature (upper axis). In each curve a jump in the enthalpy reflects the endothermic phase transition from the L_β phase to the L_α phase. The total transition enthalpy is $\Delta H \approx 11$ MJ/mol (see also Table 1), obtained from a fit to the enthalpy curves as explained below. This result is found to be independent of the heating rate, corresponds to an enthalpy per lipid of $\Delta h = \Delta H/N_l \approx 37$ kJ/mol and is in satisfactory agreement with $\Delta h \approx 33$ kJ/mol obtained in simulations of a smaller system with $N_l = 72$ lipids. These values are also in rough agreement with experimental literature values[10−12,53,54] for the enthalpy of the chain melting main transition, $\Delta h = 35-40$ kJ/mol. However, our simulations do not capture the so-called "pretransition" from the L_β phase to the P_β^* phase observed experimentally at intermediate temperatures between the L_β and the L_α phases,[3,55] because the P_β^* phase is characterized by "ripples" on lateral length scales hardly accessed in atomistic MD simulations.[30,56] Consequently, our result might more correctly be compared to the combined experimental transition enthalpy of pre- and main transition, which is about $\Delta h = 41-46$ kJ/mol, making the agreement between simulation and experiment less perfect. Future studies on this subtle detail would be desirable.

As a result of the stochastic nature of individual membrane melting events, the melting times t_m are statistically distributed (see Figure 3a), and the corresponding instantaneous temperatures at the transition are thus distributed around an average value T_m^{app}. Far from the transition, H increases virtually linearly with temperature, reflecting the approximately constant heat capacity c_p of the system in the covered temperature range. It should be noted that no significant difference in c_p below and above the melting (i.e., in L_β and L_α phases) is observed, in agreement with experimental reports for DPPC[54] and in accord with our assumption of temperature-independent transition enthalpy and entropy.

Figure 3b shows the evolution of the system enthalpy around the transition in a representative melting simulation of a bilayer with $N_l = 288$ at the highest hydration and $r = 0.125$ K/ns. At selected time points along the transition the bilayer structure is analyzed. Figure insets show the density of alkyl chain gauche bonds in one lipid monolayer as a function of the x and y coordinates in the membrane plane on a grid formed by 10 × 10 voxels. A high density of gauche bonds identifies melted membrane regions. It is seen that melting is not homogeneous but nucleates locally and propagates laterally until the melted region fills the entire simulation box and a homogeneous membrane in the L_α phase is formed. This observation of a laterally propagating phase boundary is consistent with an earlier simulation study on coexisting, prearranged L_α and L_β phases.[33] Figure 3c (main panel) shows the number of alkyl chain gauche bonds in the lower (orange line) and upper (green line) lipid monolayer around the transition. As follows from the virtually simultaneous increase in the numbers of gauche bonds in the two monolayers, both monolayers melt in a correlated way.

In principle, the coupling between the monolayers can be caused by two alternative mechanisms, due to interaction between the monolayers or via coupling to the external lateral pressure, i.e., in terms of the variable yet common membrane area in the simulation box. The black line in Figure 3c indicates the evolution of the membrane area in the same melting simulation. Its increase reflecting the phase transition occurs several nanoseconds after the increase in the number of gauche bonds in both monolayers. This observation argues against transition coupling via the constant lateral pressure boundary condition and suggests that melting of the two monolayers is coupled due to localized intermonolayer interactions. In fact, as presented in the inset of Figure 3c, the in-plane positions of melted regions in the two monolayers are correlated during early stages of the transition. Note that the transient contraction of the membrane area prior to the expansion is not always observed (see Supporting Information for other simulation runs) and therefore cannot be a central aspect of the melting mechanism. Note also that the time constant used for the pressure equilibration ($\tau_p = 0.5$ ps, see Methods and Materials section) is much shorter than the duration of the relaxation of the membrane area, so that we can exclude any related artifacts. Phase coupling between monolayers has been observed experimentally also in segregated multicomponent bilayers[57] and attributed to various physical mechanisms, based on concentration fluctuations of the components, electrostatics in charged membranes, and dynamic chain interdigitation, among others.[58] Our finding of laterally correlated fluid domains spanning both monolayers on the length scale of a nanometer in single-component membranes corroborates the importance of intermonolayer coupling mechanisms based on the lipids' short-ranged interactions involving tail conformational entropy effects.

Determination of Apparent Melting Temperatures. For a quantitative analysis of the system enthalpy kinetics in the melting simulations, a fit function is used. It consists of the sum of a linear function representing the constant heat capacity and an error function representing the phase transition

$$H(t) = H_{init} + c_p rt + \frac{\Delta H}{2}\left[1 + \mathrm{erf}\left(\frac{t - t_c}{\sqrt{2}\tau}\right)\right] \quad (20)$$

where t_c denotes the time at the center of the enthalpy jump and τ the duration of the jump. In Figure 3a a typical fit is indicated with a solid red line. The solid blue line indicates the linear baseline, given by $H(t) = H_{init} + c_p rt$. The fit function assumes identical heat capacities below and above the transition, in agreement with the simulation data. The heat capacity per lipid, c_p^l, can be estimated from the fit result for c_p employing the additivity approximation $c_p \approx N_w c_p^w + N_l c_p^l$, where $c_p^w = 0.079$ kJ/(mol K) denotes the water heat capacity in bulk TIP3P water simulations,[60] in good agreement with the experimental value of 0.075 kJ/(mol K).[61] The obtained value $c_p^l \approx 0.9$ kJ/(mol K), is significantly lower than the experimental value of 1.6 kJ/(mol K),[54] which reflects the unified-atom representation of the alkyl chains in the DPPC force field,[41] leading to a substantial reduction in the number of degrees of freedom.

The finite duration τ of the enthalpy jump results from the sum of the transition path time τ_{tp}, i.e., the time required to reach the transition state,[36] and relaxation processes after reaching the transition state, notably the propagation of the phase boundary, the velocity of which is r-dependent. As will be

DOI: 10.1021/acs.jpcb.5b05501
J. Phys. Chem. B 2015, 119, 14157−14167

Table 2. Parameters Characterizing the Thermodynamic Properties of the Transition State As Deduced from the Simulations at Various Hydration Levels n_w and System Sizes Characterized by the Number of Lipids N_l[a]

N_l	n_w	θ [10^3 K]	ln(r^* (K/ns))	ΔH^*_β [kJ/mol]	ΔS^*_β [kJ/(mol K)]	ΔG^*_β [kJ/mol] at 320 K	ΔG^*_β [$k_B T^{eq}_m$] at T^{eq}_m
288	7	33.7 ± 3.3	112 ± 10	280 ± 27	{0.70, 0.64, 0.58} ± 0.09	{56.6, 74.9, 93.3} ± 0.5	{23.6, 30.5, 37.4} ± 0.2
288	10	36.7 ± 4.0	122 ± 13	304 ± 33	{0.78, 0.72, 0.66} ± 0.11	{55.4, 73.8, 92.2} ± 0.5	{23.5, 30.4, 37.3} ± 0.2
288	31	38.3 ± 3.5	128 ± 11	318 ± 29	{0.83, 0.77, 0.71} ± 0.09	{53.7, 72.0, 90.4} ± 0.5	{23.4, 30.3, 37.3} ± 0.2
72	31	34.6 ± 5.4	115 ± 17	288 ± 45	{0.73, 0.68, 0.62} ± 0.14	{56.6, 74.7, 92.9} ± 0.7	{23.0, 29.9, 36.8} ± 0.3

[a]The values in curly brackets correspond to different choices of $k_0 \in \{10^8, 10^{11}, 10^{14}\}$ Hz. For the small system (N_l = 72) a 4-times smaller value of k_0 was considered, as required by the 4-times smaller membrane area (see main text).

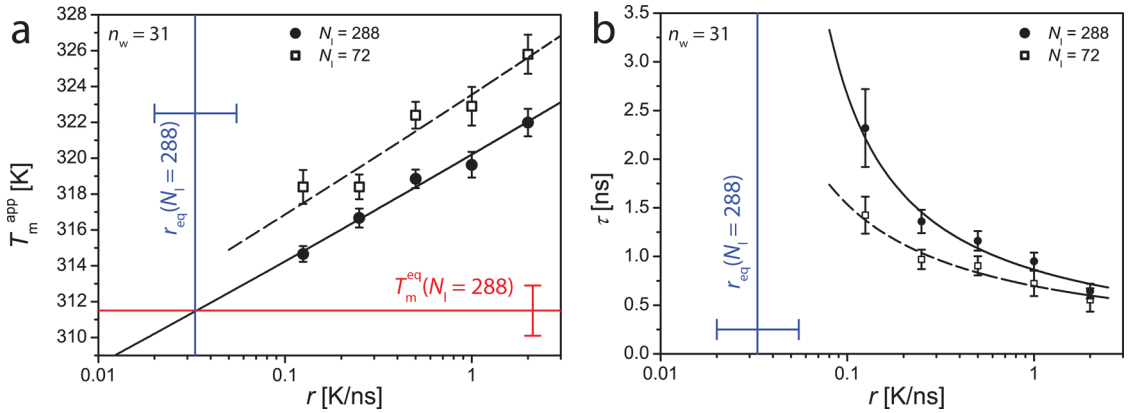

Figure 4. (a) Apparent chain melting temperatures T^{app}_m of bilayers hydrated with n_w = 31 water molecules per lipid (highest hydration) as a function of the heating rate in the simulations. Solid and dashed lines are fits of eq 16 to the data points for large (N_l = 288) and small (N_l = 72) bilayers, respectively. For the large system the plot also exemplarily indicates the characteristic heating rate r_{eq} as determined from the fit in panel b and the resulting equilibrium melting temperature T^{eq}_m. (b) Transition duration τ in dependence on the heating rate for large and small bilayers at the highest hydration. Solid and dashed lines indicate the best-matching models according to eq 23. The vertical line exemplarily indicates the best-matching value of r_{eq} for the large system.

discussed further below, the transition state is located toward the onset of the enthalpy jump and assumed to be independent of the heating rate. Accordingly, in each run the apparent melting time t_m, i.e., the time at which the transition state is reached (introduced in eqs 8 and 9), is defined as

$$t_m = t_c - x\tau \tag{21}$$

with the same x value for all rates and hydration levels. With that the transition state enthalpy ΔH^*_β can be expressed as

$$\Delta H^*_\beta = \frac{\Delta H}{2}\left[1 - \mathrm{erf}\left(\frac{x}{\sqrt{2}}\right)\right] \tag{22}$$

As explained further below, x = 1.9 and 1.2 were determined for large (N_l = 288) and small (N_l = 72) bilayers, respectively, leading to $\Delta H^*_\beta \approx$ 300 kJ/mol (see Table 2) for both system sizes, corroborating the notion of a spatially localized transition state that is independent of the system size.

The average temperature at which the membranes cross the transition state upon heating at a given heating rate r is then calculated according to eq 9 by averaging over different runs. Since refreezing events are not taken into consideration and are also not observed during the simulation time, T^{app}_m represents the average temperature of irreversible melting events. As introduced above, this scenario can be described by a two-state model assuming $k_{\alpha\beta} = 0$.

Figure 4a shows the obtained T^{app}_m as a function of r for bilayers at the highest hydration (N_w = 31) with N_l = 288 and 72. Each data point represents the average of 7−15 independent heating simulations. The error bars represent the corresponding standard errors and reflect the statistical distribution of t_m. Straight lines in the semilogarithmic plot indicate logarithmic fits to the data and illustrate that T^{app}_m increases logarithmically with r. According to eqs 14−18, the $T^{app}_m(r)$ data obtained in the simulations contain information on the transition state, as characterized by ΔH^*_β and ΔS^*_β. These two quantities are obtained by fitting T_0 and C in eq 16 to the simulation data points and subsequent conversion using eqs 14−18. For the large bilayer we obtain ln(r^* (K/ns)) = 128 ± 11 and θ = (38.3 ± 3.5) × 10^3 K. As shown in the Supporting Information, consistent results are obtained using a classical Kissinger plot approach.

Values of comparable magnitude are obtained for all hydration levels and also for the small system, see also Table 2. (Small but distinct differences between the different systems are discussed further below.) According to eq 14, the corresponding transition state enthalpies $\Delta H^*_\beta = k_B\theta$ are of the order of 300 kJ/mol. The dependence of this result on the choice of x in eq 21 is illustrated in Figure 5 exemplarily for the large system at the highest hydration. The blue line indicates ΔH^*_β as obtained in the described way from $T^{app}_m(r)$ data generated for x-dependent definitions of t_m in eq 21. It is seen that the result is only mildly dependent on x. The red line is $\Delta H^*_\beta(x)$ as defined by eq 22. The intersection of red and blue curves defines the value of x = 1.9 for the large systems, in which ΔH^*_β corresponds to about 3% of the enthalpy difference between L_α and L_β phase, $\Delta H^*_\beta \approx 0.03\Delta H$. Analogous reasoning leads to x = 1.2 for the small system, in which case $\Delta H^*_\beta \approx 0.12\Delta H$.

Estimation of Equilibrium Melting Temperatures. Figure 4b shows the transition duration τ in dependence on the heating rate for both system sizes (N_l = 288 and 72) at the

DOI: 10.1021/acs.jpcb.5b05501
J. Phys. Chem. B 2015, 119, 14157−14167

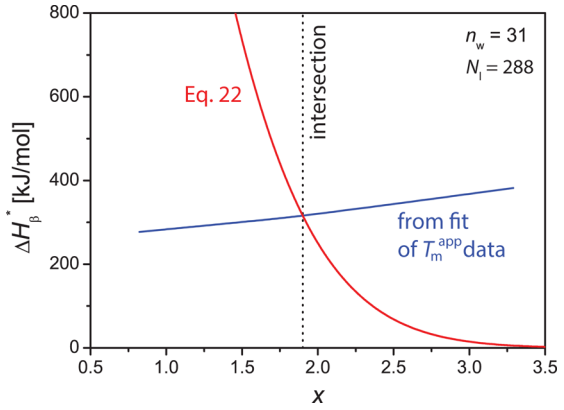

Figure 5. ΔH_β^* for the large bilayer at the highest hydration as obtained in fits of the T_m^{app} data according to eq 16 for t_m as defined in eq 21 (blue line) and ΔH_β^* as defined in eq 22 (red line). The intersection of the two curves defines x = 1.9 for the large systems.

highest hydration (n_w = 31). We find that τ systematically decreases with increasing heating rate. This behavior can be rationalized in the following way: After nucleation, the phase boundary propagates along the simulation box with a finite, temperature-dependent velocity, v, and the time required for the complete propagation of the newly formed phase throughout the entire system is inversely proportional to v. Experiments[18] suggested that the leading term in a Taylor expansion of $v(T)$ is linear, so that v scales as $(T - T_m^{eq})$ in the vicinity of T_m^{eq}, consistent with a previous MD simulation study.[33] In the present study the instantaneous temperature at which the phase transition occurs on average for a given heating rate is T_m^{app}. According to eq 19, $(T_m^{app} - T_{eq})$ approximately scales as $\ln(r/r_{eq})$, so that we obtain $v \propto \ln(r/r_{eq})$. On the basis of these considerations we model the transition duration as a whole as

$$\tau(r) = \tau_0 + \frac{A}{\ln(r/r_{eq})} \tag{23}$$

with adjustable parameters τ_0, A, and r_{eq}. The constant (i.e., rate-independent) contribution τ_0 is introduced to account for other contributions to τ, which depend weakly on r when compared to the propagation of the phase boundary, notably the transition path time τ_{tp} (see Supporting Information for a discussion of τ_{tp}'s r dependence). As shown in Figure 4b, eq 23 reproduces $\tau(r)$ well. Solid and dashed lines indicate the models corresponding to the best-matching parameter sets for large and small systems, respectively. For the large system we obtain $\ln(r_{eq}\ (\mathrm{K/ns})) = -3.4 \pm 0.5$ (and on the linear scale 0.020 K/ns < r_{eq} < 0.055 K/ns, best-matching value r_{eq} = 0.033 K/ns), where the error bar is derived from the diagonal elements of the parameter covariance matrix.[62] For the constant term we obtain $\tau_0 \approx 0$, with a statistical error of 0.26 ns. As

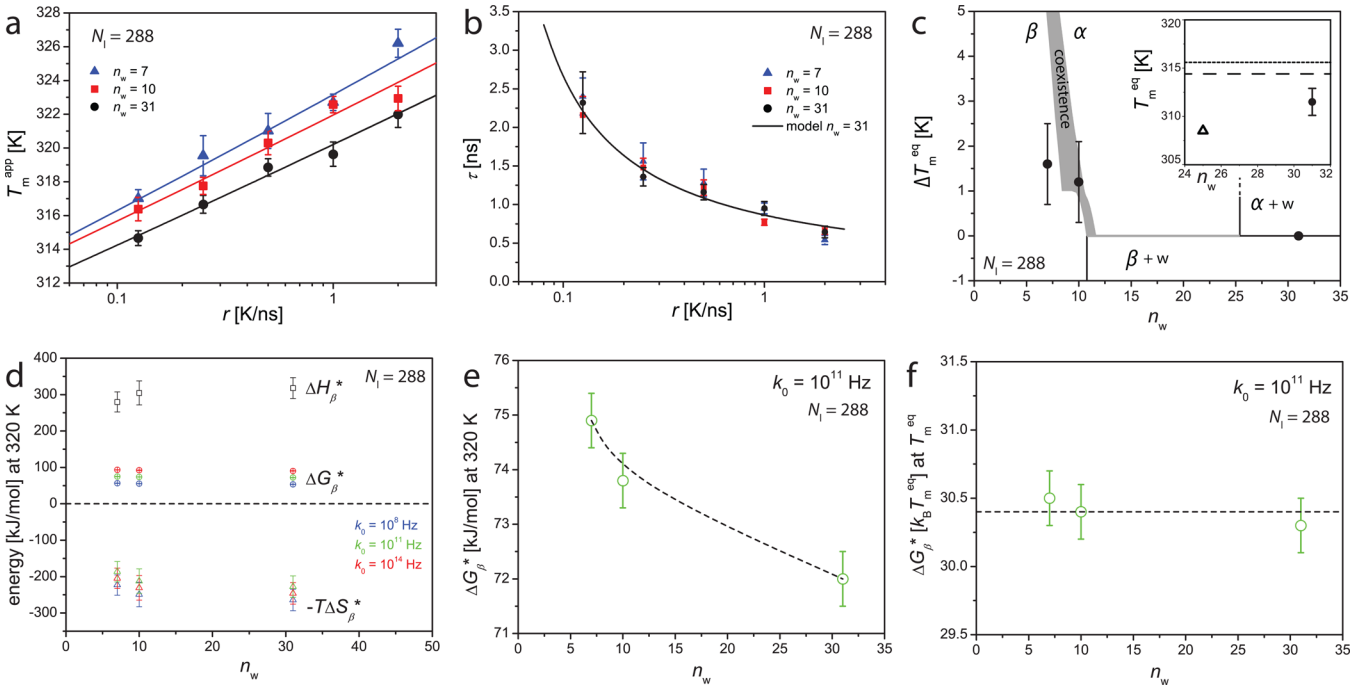

Figure 6. (a) Apparent chain melting temperatures T_m^{app} of bilayers formed by N_l = 288 DPPC molecules as a function of r for different hydration levels n_w. Solid lines are fits according to eq 16. (b) Transition durations τ as a function of r for different hydration levels. Data points for different hydration levels are consistent with the best-matching model (solid line) obtained for n_w = 31 (see Figure 4b). (c) Shift of the equilibrium melting temperature upon dehydration, ΔT_m^{eq}. Simulation results for different hydration levels (symbols) are compared with the relevant region of the DPPC/water phase diagram. See main text for details on the error bars. Shaded area indicates coexistence of fluid (α) and gel (β, L_β, or P_β) phases established experimentally by Ulmius et al.[59] Vertical black lines schematically indicate the hydration levels above which pure gel and fluid phases coexist with excess water β + w and α + w, respectively. (Inset) Equilibrium melting temperature T_m^{eq} for the highest hydration level (filled circle) together with the melting temperatures for excess hydration determined experimentally by Grabielle-Madelmont et al.[15] (lower dashed line) and Ulmius et al.[59] (upper dotted line). The triangle indicates the result of an earlier simulation study at n_w = 25 using SPC water.[33] (d) Transition state free energy ΔG_β^* at a fixed reference temperature T = 320 K and its enthalpic and entropic contributions, obtained from eqs 14 and 15, respectively, for several choices of the transition attempt frequency k_0 and as a function of n_w. (e) Closeup view on ΔG_β^* at T = 320 K. (f) Closeup view on ΔG_β^* at T_m^{eq} in units of $k_B T_m^{eq}$. Dashed lines in panels e and f serve as guides to the eye.

DOI: 10.1021/acs.jpcb.5b05501
J. Phys. Chem. B 2015, 119, 14157−14167

shown in the previous section, the transition state is located at the very onset of the enthalpy jump. The immeasurably small value of τ_0 is consistent with this expectation. For the small system we obtain $\ln(r_{eq}\ (\mathrm{K/ns})) = -4.2 \pm 1.2$ (0.005 K/ns < r_{eq} < 0.050 K/ns). The best-matching value (r_{eq} = 0.015 K/ns) is about two times lower for the small system than for the large system. However, within the given error range our results are consistent with the theoretically expected factor of 4, which corresponds to the size ratio between large (N_l = 288) and small (N_l = 72) systems, namely, each portion of the bilayer contributes independently to the melting attempt frequency k_0 (introduced in eqs 5 and 6), so that k_0 and $r_{eq} \propto k_0$ should scale with the bilayer surface. In Figure 4a and 4b r_{eq} is indicated exemplarily for the large bilayer.

At this point we recall that by definition r_{eq} is the characteristic heating rate for which $T_m^{app} = T_m^{eq}$, so that T_m^{eq} is obtained by inserting r_{eq} into eq 12 (or, equivalently, into eq 16). For the large and small bilayers at the highest hydration we obtain T_m^{eq} = 311.5 ± 1.4 and 311.5 ± 3.5 K, respectively, where the error bars account for the uncertainties in r_{eq}, θ, and r^* (see also Table 1). In Figure 4a, T_m^{eq} is indicated exemplarily for the large system. The obtained equilibrium melting temperature is similar to the one reported earlier in an MD simulation study on DPPC for n_w = 25 with a different water model (T_m^{eq} = 308.5 K)[33] and is in remarkable agreement with the known experimental value at excess hydration, $T_m^{eq} \approx 315$ K.[15,59] An overview of these results is shown in the inset of Figure 6c. Our simulations at the highest hydration level do not correspond to lamellar phases at excess hydration but, as mentioned further above, rather represent the melting behavior of large isolated membranes. However, since experiments have shown that there is no significant difference between the chain melting transition temperature in unilamellar and multilamellar DPPC vesicles in excess water,[13,63] our results at n_w = 31 may be equally compared to experimental data from large unilamellar vesicles and multilamellar systems in excess water. In fact, as derived in the theoretical literature,[64,65] the phase diagram depends on the mutual membrane interactions in the lamellae. Since the magnitude of these interactions at the swelling limit in both phases is very low, its influence on the transition temperature is minor. With that the experimentally observed virtually identical chain melting temperatures of large unilamellar and multilamellar membrane systems are also expected from a theoretical viewpoint. The good agreement between simulation and experiment is somewhat surprising, because the lipid force field was optimized with respect to other characteristics, such as area per lipid in the L_α phase, which are accessible in simulations more easily.[41]

The value for T_m^{eq} obtained here together with the phase transition enthalpies determined above yield $\Delta S = \Delta H/T_m^{eq}$ = 34.9 ± 0.3 and 7.6 ± 0.5 kJ/(mol K) for the large and small bilayers, respectively, at the highest hydration, corresponding to an entropy per lipid of about $\Delta s = \Delta S/N_l \approx 100-120$ J/(mol K) (see Table 1).

Thermodynamic Characterization of the Transition State. In the section where we discussed the apparent melting temperature the transition state enthalpy of the large bilayer (N_l = 288) at the highest hydration was determined as $\Delta H_\beta^* \approx 300$ kJ/mol (see Table 2). The transition state entropy ΔS_β^* is defined by θ and r^* only up to the unknown value of the transition attempt frequency k_0 (see eq 15). However, we can safely assume that 10^8 Hz < k_0 < 10^{14} Hz, where the range is limited by the duration and by the time step of the MD simulations capturing the melting process. With that ΔS_β^* is determined up to an unknown offset which is comparable to the statistical error. We obtain ΔS_β^* = 0.71 ± 0.09 kJ/(mol K) at $k_0 = 10^{14}$ Hz, ΔS_β^* = 0.77 ± 0.09 kJ/(mol K) at $k_0 = 10^{11}$ Hz, and ΔS_β^* = 0.83 ± 0.09 kJ/(mol K) at $k_0 = 10^8$ Hz (see also Table 2). The statistical precision with which the fit determines ΔG_β^* is much greater than in the case of ΔH_β^* and ΔS_β^*. This is because the errors in ΔH_β^* and ΔS_β^* are strongly anticorrelated. Nonetheless, the systematic, k_0-related uncertainty in ΔS_β^* is propagated also to ΔG_β^*. Close to the transition temperature the enthalpic term is significantly more positive than the entropic term is negative, so that ΔG_β^* is significantly positive, between ∼55 and ∼92 kJ/mol at T = 320 K, depending on the choice of k_0, see Table 2. (T = 320 K was chosen exemplarily as it roughly coincides with the center of the sampled data range.) In other words, there is a sizable free energy barrier because the transition state entropy with respect to the L_β phase does not increase sufficiently to compensate for the corresponding enthalpy increase.

Another important observation is that while ΔH and ΔS scale with the system size (identified by N_l, see Table 1), ΔH_β^* and ΔS_β^* are virtually independent of the system size (see Table 2). This result clearly rules out a transition state that involves all lipids in the simulation box, as in that case ΔH_β^* and ΔS_β^* would also be proportional to N_l. In other words, the transition state must be considered a localized nucleus. This conclusion is consistent with the observation that the phase transition is initiated by a localized structural perturbation which then propagates through the membrane plane (see Figure 3b). However, the thermodynamic characterization performed in the previous section puts us in the position to draw a more detailed picture: If we express the transition state enthalpy as a multiple n_l of the transition enthalpy per lipid, $\Delta H_\beta^* = n_l \Delta h$ then we obtain $n_l \approx 8$. If we repeat the same with the transition state entropy, we obtain $n_l = \Delta S_\beta^*/\Delta s \approx 5-7$, depending on the chosen value of k_0. The order of magnitude of n_l defines the approximate size of the melting nucleus, which is in fact consistent with a previous experimental estimate of 7 lipids as the minimum nucleation size in DPPC bilayers.[18] The small but distinct difference between n_l as deduced from the enthalpy and n_l as deduced from the entropy, on the other hand, yields insight into the properties of the nucleus: The lipids involved in the nucleation assume configurations which are more unfavorable enthalpically than they are favorable entropically. In other words the transition state constitutes a free energy barrier because, as the system moves along the reaction coordinate toward the melted state, lipids first have to give up favorable enthalpic interactions before this is again compensated by a gain in entropy. To our knowledge this is the first time that the melting nucleation in lipid bilayers has been quantitatively characterized in thermodynamic and structural terms.

Influence of the Hydration Level. Experiments on multibilayers formed by phosphatidylcholine lipids with saturated hydrocarbon chains have revealed that the systems' phase behavior is affected substantially by dehydration: As illustrated in Figure 6c, macroscopic lamellar systems containing a fixed amount of water below the swelling limit of the fluid phase at around 25 water molecules per lipid exhibit two-phase gel/fluid coexistence above the main transition temperature. In the figure α denotes the fluid phase and β denotes the gel phase (L_β or P_β). For higher water contents, excess water coexists with either pure gel (β + w) or pure fluid

DOI: 10.1021/acs.jpcb.5b05501
J. Phys. Chem. B 2015, 119, 14157−14167

phases (α + w), depending on the temperature.[64] Importantly, the temperatures of the $\alpha-\beta$ phase coexistence boundaries increase upon dehydration. In other words, dehydration is known to stabilize the gel phase with respect to the fluid phase.[13−15,59] In order to study this effect in MD simulations we realized and investigated two additional large bilayer systems with lower hydration levels of n_w = 10 and 7 water molecules per lipid, in addition to the above-discussed systems with n_w = 31.

Figure 6a shows $T_m^{app}(r)$ for N_l = 288 at all three hydration degrees. Lines indicate the best-matching models according to eq 16. The corresponding parameters θ and r^* are summarized in Table 2. Throughout the studied range of heating rates we observe a systematic increase of T_m^{app} by about 2 K as the bilayers get dehydrated from n_w = 31 via n_w= 10 to n_w= 7. According to eq 19 this requires that either T_m^{eq} or r_{eq}, or both, depend on n_w (For fixed T_m^{eq} and r_{eq}, variations in θ merely change the slope of $T_m^{app}(r)$ in the semilogarithmic Figure 6a, and θ is found not to depend significantly on n_w, see Table 2). As shown in Figure 6b, the transition duration τ is largely independent of n_w, so that r_{eq} as determined above for n_w = 31 also applies to the dehydrated bilayers. This necessarily implies that the shift in $T_m^{app}(r)$ mainly reflects a corresponding shift in T_m^{eq}. Calculating T_m^{eq} along the line discussed above for n_w = 31 yields $T_m^{eq}(n_w = 10)$ = 312.6 ± 1.5 K and $T_m^{eq}(n_w = 7)$ = 313.1 ± 1.6 K (see Table 1). The main panel of Figure 6c shows the shift of the equilibrium melting temperature upon dehydration, $\Delta T_m^{eq}(n_w)$. Simulation results for different hydration levels (symbols) are compared with the relevant region of the DPPC/water phase diagram. The shaded area indicates coexistence of fluid (α) and gel (β, L_β, or P_β) phases as established experimentally by Ulmius et al.[59] For hydration levels above n_w = 12, roughly coinciding with the swelling limit of the gel phase, the temperature width of the coexistence region is very small. In the figure, coexistence in this hydration range is therefore indicated only schematically with a horizontal gray line up to the triple point at the swelling limit of the fluid phase. Note, however, that the temperature range of the coexistence region increases with decreasing hydration.[64] It is seen that the increase of the chain melting temperature in the simulations with decreasing hydration level is in qualitative agreement with the hydration dependence of the lower and upper boundaries of the coexistence region. While it is difficult to define to which part of the coexistence region the simulation results should be compared most correctly, we note that the phase coexistence region is only about 1−2 water molecules per lipid wide along the n_w axis, which means that the hydration levels in the two phases are not very different throughout coexistence. In other words, the fact that the simulations by construction cannot capture the phase coexistence regime effectively translates into an uncertainty of the hydration level by only 1−2 water molecules per lipid. The values of ΔT_m^{eq} are also summarized in Table 1. Note that the corresponding error bars are significantly smaller than those of T_m^{eq}. This is because r_{eq} can be assumed to be hydration-independent, as suggested by Figure 6b. The error associated with r_{eq} thus equally affects the data points for all hydration levels and therefore can be neglected when merely looking at incremental changes.

The parameters characterizing the thermodynamic properties of the transition state for all hydration levels and system sizes are summarized in Table 2. In Figure 6d the transition state free energy ΔG_β^* at 320 K and its enthalpic and entropic terms, ΔH_β^* and $-T_m^{eq}\Delta S_\beta^*$, respectively, are plotted as functions of n_w. In tendency, ΔH_β^* increases slightly with n_w, while the entropic term also slightly increases in magnitude, but these trends are not significant in view of the statistical errors. For the more precisely determined barrier height ΔG_β^* in Figure 6e, however, we observe a systematic increase with decreasing hydration level. This means that, on an absolute temperature scale, dehydration increases the free-energy barrier between the L_β and the L_α phases. This trend disappears, however, when the barrier heights are compared with each other at their respective transition temperatures and plotted in units of $k_B T_m^{eq}$ (Figure 6f). In other words, while dehydration significantly shifts the equilibrium chain melting temperature with important biological implications, the transition state itself remains qualitatively unaffected.

CONCLUSION

The phase behavior of lipid membranes is biologically important, for instance, for the formation of functional lipid domains, membrane permeability, and mechanical properties.[3,66] It is well established that the chain melting phase transition depends on many parameters out of which the hydration is of particular interest because it has immediate consequences for the function and permeability of the skin.[6] In the present study we determined the structural and thermodynamical characteristics of the phospholipid membrane chain melting transition in dependence on the hydration level. Our computer simulations reproduce the experimentally observed stabilization of the gel phase with respect to the fluid phase upon dehydration, which has previously been rationalized in terms of interfacial forces and the phase-dependent average membrane area occupied per lipid molecule.[6] The present simulation results for the first time provide thermodynamic and structural detail of the chain melting transition and together with atomistic simulations of interfacial forces between membranes[28,67] may contribute to a better understanding of the effects of dehydration. Our approach can be readily extended for the study of other biologically relevant parameters affecting the phase behavior of lipid bilayers, for instance, the membrane composition, ions in the aqueous medium, or small polar molecules that act as moisturizers.[16] The simulations are then likely to reveal the physical mechanisms leading to a shift in the transition temperature and the potential impact on the transition state. The theoretical concepts presented are applicable not only to membrane phase transitions but also to thermal protein unfolding and other problems involving thermotropic phase transitions.

ASSOCIATED CONTENT

Supporting Information

The Supporting Information is available free of charge on the ACS Publications website at DOI: 10.1021/acs.jpcb.5b05501.

Derivation of eq 12; derivation of eqs 16 and 19; heating rate dependence of the transition path time; determination of θ and r^* via the Kissinger method; evolution of membrane area and number of gauche bonds for several heating runs (PDF)

AUTHOR INFORMATION

Corresponding Author

*E-mail: schneck@mpikg.mpg.de.

DOI: 10.1021/acs.jpcb.5b05501
J. Phys. Chem. B 2015, 119, 14157−14167

Notes

The authors declare no competing financial interest.

■ ACKNOWLEDGMENTS

We gratefully acknowledge support by the DFG grant SFB 1112 and computing time on the HELICS II clusters (University of Heidelberg), bwGRiD (http://www.bw-grid.de, member of the German DGrid initiative), and Leibniz Rechenzentrum München (LRZ project pr28xe). We thank David A. Pink, Gregor Cevc, and Luca Bertinetti for insightful comments. E.S. acknowledges support from a Marie Curie Intra-European Fellowship within the European Commission seventh Framework Program and from an Emmy-Noether grant (SCHN 1396/1) of the German Research Foundation (DFG).

■ REFERENCES

(1) Singer, S. J.; Nicolson, G. L. The fluid mosaic model of the structure of cell membranes. *Science* **1972**, *175*, 720−731.
(2) Cevc, G.; Marsh, D. *Phospholipid bilayers: physical principles and models*; Wiley, 1987; Vol. *5*.
(3) Lipowsky, R.; Sackmann, E. *Structure and Dynamics of Membranes: I. From Cells to Vesicles/II. Generic and Specific Interactions*; Access Online via Elsevier, 1995; Vol. *1*.
(4) Mouritsen, O. G. *Life - As a Matter of Fat*; Springer,2005.
(5) Bloom, M.; Evans, E.; Mouritsen, O. G. Physical properties of the fluid lipid-bilayer component of cell membranes: a perspective. *Q. Rev. Biophys.* **1991**, *24*, 293−397.
(6) Sparr, E.; Wennerström, H. Responding phospholipid membranes-interplay between hydration and permeability. *Biophys. J.* **2001**, *81*, 1014−1028.
(7) Nagle, J. F.; Tristram-Nagle, S. Structure of lipid bilayers. *Biochim. Biophys. Acta, Rev. Biomembr.* **2000**, *1469*, 159.
(8) Kucerka, N.; Tristram-Nagle, S.; Nagle, J. F. Closer Look at Structure of Fully Hydrated Fluid Phase DPPC Bilayers. *Biophys. J.* **2006**, *90*, L83.
(9) Tristram-Nagle, S.; Zhang, R.; Suter, R.; Worthington, C.; Sun, W.; Nagle, J. Measurement of chain tilt angle in fully hydrated bilayers of gel phase lecithins. *Biophys. J.* **1993**, *64*, 1097−1109.
(10) Biltonen, R. L. A statistical-thermodynamic view of cooperative structural changes in phospholipid bilayer membranes: their potential role in biological function. *J. Chem. Thermodyn.* **1990**, *22*, 1−19.
(11) Mabrey, S.; Sturtevant, J. M. Investigation of phase transitions of lipids and lipid mixtures by high sensitivity differential scanning calorimetry. *Proc. Natl. Acad. Sci. U. S. A.* **1976**, *73*, 3862−3866.
(12) Janiak, M. J.; Small, M. D.; Shipley, G. G. Nature of the thermal pretransition of synthetic phospholipids: dimyristoyl- and dipalmitoyllecithin. *Biochemistry* **1976**, *15*, 4575.
(13) Koynova, R.; Caffrey, M. Phases and phase transitions of the phosphatidylcholines. *Biochim. Biophys. Acta, Rev. Biomembr.* **1998**, *1376*, 91−145.
(14) Jürgens, E.; Höhne, G.; Sackmann, E. Calorimetric Study of the Dipalmitoylphosphatidylcholine/ Water Phase Diagram. *Ber. Bunsenges. Phys. Chem.* **1983**, *87*, 95−104.
(15) Grabielle-Madelmont, C.; Perron, R. Calorimetric studies on phospholipid-water systems: I. dl-Dipalmitoylphosphatidylcholine (DPPC)-water system. *J. Colloid Interface Sci.* **1983**, *95*, 471−482.
(16) Costa-Balogh, F. O.; Wennerström, H.; Wadsö, L.; Sparr, E. How small polar molecules protect membrane systems against osmotic stress: the urea-water-phospholipid system. *J. Phys. Chem. B* **2006**, *110*, 23845−23852.
(17) Kharakoz, D.; Colotto, A.; Lohner, K.; Laggner, P. Fluid-gel interphase line tension and density fluctuations in dipalmitoylphosphatidylcholine multilamellar vesicles: an ultrasonic study. *J. Phys. Chem.* **1993**, *97*, 9844−9851.
(18) Kharakoz, D. P.; Shlyapnikova, E. A. Thermodynamics and kinetics of the early steps of solid-state nucleation in the fluid lipid bilayer. *J. Phys. Chem. B* **2000**, *104*, 10368−10378.
(19) Frenkel, J. A general theory of heterophase fluctuations and pretransition phenomena. *J. Chem. Phys.* **1939**, *7*, 538.
(20) Spaepen, F. Homogeneous nucleation and the temperature dependence of the crystalmelt interfacial tension. *Solid State Phys.* **1994**, *47*, 1.
(21) Vehkamäki, H. *Classical nucleation theory in multicomponent systems*; Springer: Berlin Heidelberg, 2006.
(22) Mouritsen, O. Theoretical models of phospholipid phase transitions. *Chem. Phys. Lipids* **1991**, *57*, 179−194.
(23) Nagle, J. F. Theory of the main lipid bilayer phase transition. *Annu. Rev. Phys. Chem.* **1980**, *31*, 157−196.
(24) Mouritsen, O.; Boothroyd, A.; Harris, R.; Jan, N.; Lookman, T.; MacDonald, L.; Pink, D.; Zuckermann, M. Computer simulation of the main gel-fluid phase transition of lipid bilayers. *J. Chem. Phys.* **1983**, *79*, 2027.
(25) Jämbeck, J. P.; Lyubartsev, A. P. Derivation and systematic validation of a refined all-atom force field for phosphatidylcholine lipids. *J. Phys. Chem. B* **2012**, *116*, 3164−3179.
(26) Marrink, S.-J.; Berendsen, H. J. Simulation of water transport through a lipid membrane. *J. Phys. Chem.* **1994**, *98*, 4155−4168.
(27) de Vries, A. H.; Chandrasekhar, I.; van Gunsteren, W. F.; Hünenberger, P. H. Molecular dynamics simulations of phospholipid bilayers: Influence of artificial periodicity, system size, and simulation time. *J. Phys. Chem. B* **2005**, *109*, 11643−11652.
(28) Schneck, E.; Sedlmeier, F.; Netz, R. R. Hydration repulsion between biomembranes results from an interplay of dehydration and depolarization. *Proc. Natl. Acad. Sci. U. S. A.* **2012**, *109*, 14405−14409.
(29) Leekumjorn, S.; Sum, A. K. Molecular studies of the gel to liquid-crystalline phase transition for fully hydrated DPPC and DPPE bilayers. *Biochim. Biophys. Acta, Biomembr.* **2007**, *1768*, 354−365.
(30) Schubert, T.; Schneck, E.; Tanaka, M. First Order Melting Transitions of Highly Ordered DPPC Gel Phase Membranes in Molecular Dynamics Simulations with Atomistic Detail. *J. Chem. Phys.* **2011**, *135*, 055105.
(31) Venable, R. M.; Brooks, B. R.; Pastor, R. W. Molecular dynamics simulations of gel ($L_{\beta}I$) phase lipid bilayers in constant pressure and constant surface area ensembles. *J. Chem. Phys.* **2000**, *112*, 4822−4832.
(32) Coppock, P. S.; Kindt, J. T. Atomistic simulations of mixed-lipid bilayers in gel and fluid phases. *Langmuir* **2009**, *25*, 352−359.
(33) Coppock, P. S.; Kindt, J. T. Determination of phase transition temperatures for atomistic models of lipids from temperature-dependent stripe domain growth kinetics. *J. Phys. Chem. B* **2010**, *114*, 11468−11473.
(34) Geiger, P.; Dellago, C. Neural networks for local structure detection in polymorphic systems. *J. Chem. Phys.* **2013**, *139*, 164105.
(35) Kumar, S.; Rosenberg, J. M.; Bouzida, D.; Swendsen, R. H.; Kollman, P. A. The weighted histogram analysis method for free-energy calculations on biomolecules. I. The method. *J. Comput. Chem.* **1992**, *13*, 1011−1021.
(36) Chung, H. S.; Louis, J. M.; Eaton, W. A. Experimental determination of upper bound for transition path times in protein folding from single-molecule photon-by-photon trajectories. *Proc. Natl. Acad. Sci. U. S. A.* **2009**, *106*, 11837−11844.
(37) Onuchic, J. N.; Luthey-Schulten, Z.; Wolynes, P. G. Theory of protein folding: the energy landscape perspective. *Annu. Rev. Phys. Chem.* **1997**, *48*, 545−600.
(38) Godoy-Ruiz, R.; Henry, E. R.; Kubelka, J.; Hofrichter, J.; Munoz, V.; Sanchez-Ruiz, J. M.; Eaton, W. A. Estimating free-energy barrier heights for an ultrafast folding protein from calorimetric and kinetic data. *J. Phys. Chem. B* **2008**, *112*, 5938−5949.
(39) Hess, B.; Kutzner, C.; van der Spoel, D.; Lindahl, E. GROMACS 4: Algorithms for Highly Efficient, Load-Balanced, and Scalable Molecular Simulation. *J. Chem. Theory Comput.* **2008**, *4*, 435.
(40) Tieleman, D.; Berendsen, H. J. C. Molecular dynamics simulations of a fully hydrated dipalmitoyl phosphatidylcholine bilayer

DOI: 10.1021/acs.jpcb.5b05501
J. Phys. Chem. B 2015, 119, 14157−14167

with different macroscopic boundary conditions and parameters. *J. Chem. Phys.* **1996**, *105*, 4871.
(41) Berger, O.; Edholm, O.; Jahnig, F. Molecular dynamics simulations of a fluid bilayer of dipalmitoylphosphatidylcholine at full hydration, constant pressure, and constant temperature. *Biophys. J.* **1997**, *72*, 2002.
(42) Lindahl, E.; Edholm, O. Mesoscopic Undulations and Thickness Fluctuations in Lipid Bilayers from Molecular Dynamics Simulations. *Biophys. J.* **2000**, *79*, 426−433.
(43) Jorgensen, W. L.; Chandrasekhar, J.; Madura, J. D.; Impey, R. W.; Klein, M. Comparison of simple potential functions for simulating liquid water. *J. Chem. Phys.* **1983**, *79*, 926.
(44) Berendsen, H. J. C.; Postma, J. P. M.; van Gunsteren, W. F.; DiNola, A.; Haak, J. R. Molecular dynamics with coupling to an external bath. *J. Chem. Phys.* **1984**, *81*, 3684.
(45) Darden, T.; York, D.; Pedersen, L. Particle mesh Ewald: An N log(N) method for Ewald sums in large systems. *J. Chem. Phys.* **1993**, *98*, 10089.
(46) Essmann, U.; Perera, L.; Berkowitz, M. L.; Darden, T.; Lee, H.; Pedersen, L. G. A smooth particle mesh Ewald method. *J. Chem. Phys.* **1995**, *103*, 8577.
(47) Kissinger, H. E. Reaction kinetics in differential thermal analysis. *Anal. Chem.* **1957**, *29*, 1702−1706.
(48) Farjas, J.; Roura, P. Modification of the Kolmogorov−Johnson-Mehl−Avrami rate equation for non-isothermal experiments and its analytical solution. *Acta Mater.* **2006**, *54*, 5573−5579.
(49) Corless, R. M.; Gonnet, G. H.; Hare, D. E. G.; Jeffrey, D. J.; Knuth, D. E. On the LambertW function. *Adv. Comput. Math.* **1996**, *5*, 329−359.
(50) Bell, G. I. Models for the specific adhesion of cells to cells. *Science* **1978**, *200*, 618.
(51) Evans, E.; Ritchie, K. Dynamic strength of molecular adhesion bonds. *Biophys. J.* **1997**, *72*, 1541.
(52) Rief, M.; Gautel, M.; Oesterhelt, F.; Fernandez, J. M.; Gaub, H. E. Reversible Unfolding of Individual Titin Immunoglobulin Domains by AFM. *Science* **1997**, *276*, 1109.
(53) Hinz, H.-J.; Sturtevant, J. M. Calorimetric studies of dilute aqueous suspensions of bilayers formed from synthetic L-α-lecithins. *J. Biol. Chem.* **1972**, *247*, 6071−6075.
(54) Blume, A. Apparent molar heat capacities of phospholipids in aqueous dispersion. Effects of chain length and head group structure. *Biochemistry* **1983**, *22*, 5436−5442.
(55) Sun, W.; Tristram-Nagle, S.; Suter, R. M.; Nagle, J. F. Structure of the ripple phase in lecithin bilayers. *Proc. Natl. Acad. Sci. U. S. A.* **1996**, *93*, 7008−7012.
(56) de Vries, A. H.; Yefimov, S.; Mark, A. E.; Marrink, S. J. Molecular structure of the lecithin ripple phase. *Proc. Natl. Acad. Sci. U. S. A.* **2005**, *102*, 5392−5396.
(57) Garg, S.; Rühe, J.; Lüdtke, K.; Jordan, R.; Naumann, C. A. Domain Registration in Raft-Mimicking Lipid Mixtures Studied Using Polymer-Tethered Lipid Bilayers. *Biophys. J.* **2007**, *92*, 1263−1270.
(58) May, S. Trans-monolayer coupling of fluid domains in lipid bilayers. *Soft Matter* **2009**, *5*, 3148−3156.
(59) Ulminus, J.; Wennerstrom, H.; Lindblom, G.; Arvidson, G. Deuteron nuclear magnetic resonance studies of phase equilibriums in a lecithin-water system. *Biochemistry* **1977**, *16*, 5742−5745.
(60) Vega, C.; Abascal, J. L. Simulating water with rigid non-polarizable models: a general perspective. *Phys. Chem. Chem. Phys.* **2011**, *13*, 19663−19688.
(61) Ginnings, D. C.; Furukawa, G. T. Heat Capacity Standards for the Range 14 to 1200 degrees K. *J. Am. Chem. Soc.* **1953**, *75*, 522−527.
(62) Bevington, P. R.; Robinson, D. K. *Data reduction and error analysis for the physical sciences*; McGraw-Hill: New York, 1969; Vol. *336*.
(63) Parente, R. A.; Lentz, B. R. Phase behavior of large unilamellar vesicles composed of synthetic phospholipids. *Biochemistry* **1984**, *23*, 2353−2362.
(64) Guldbrand, L.; Jönsson, B.; Wennerstrom, H. Hydration forces and phase equilibria in the dipalmitoyl phosphatidylcholine-water system. *J. Colloid Interface Sci.* **1982**, *89*, 532−541.
(65) Goldstein, R. E.; Leibler, S. Model for Lamellar Phases of Interacting Lipid Membranes. *Phys. Rev. Lett.* **1988**, *61*, 2213−2216.
(66) Griesbauer, J.; Bössinger, S.; Wixforth, A.; Schneider, M. Propagation of 2D pressure pulses in lipid monolayers and its possible implications for biology. *Phys. Rev. Lett.* **2012**, *108*, 198103.
(67) Kanduc, M.; Schneck, E.; Netz, R. R. Hydration interaction between phospholipid membranes: insight into different measurement ensembles from atomistic molecular dynamics simulations. *Langmuir* **2013**, *29*, 9126−9137.

DOI: 10.1021/acs.jpcb.5b05501
J. Phys. Chem. B 2015, 119, 14157−14167